2014

The Effect Of Type-III Antifreeze Proteins (AFPs) On CO2 Hydrate Slurry Formation

Hongxia Zhou
Delft University of Technology, Netherlands, The, h.zhou-1@tudelft.nl

Carlos A. Infante Ferreira
Delft University of Technology, Netherlands, The, C.A.InfanteFerreira@tudelft.nl

The effect of Type-III Antifreeze Proteins (AFPs) on CO_2 hydrate slurry formation

Hongxia ZHOU *, Carlos INFANTE FERREIRA

Delft University of Technology, Department Process & Energy
Delft, NL 2628 CB 39, The Netherlands
h.zhou-1@tudelft.nl
* Corresponding Author

ABSTRACT

CO_2 hydrate slurry is a favourable direct coolant of fresh products due to its large latent heat and phase change temperature around 5°C. Continuous production of this slurry is, however, difficult to realise due to the high rate of hydrate formation. The use of additives is proposed with the purpose of decreasing the formation rate so that the controllability of the process is improved. Type-III Antifreeze Proteins (AFPs) are non-poisonous additives which have proven to be inhibitors of hydrate formation. These additives have also shown to protect the bio-cells of fresh products from damaging by freezing. The effect of these additives on the CO_2 hydrate formation rate is experimentally investigated.

The experiments have been performed in a coil heat exchanger with 6 mm internal diameter under operating conditions corresponding to hydrate formation conditions. The concentration of Type-III AFPs has been varied: no additives, 5 ppm and 10 ppm. The mixture of additives and CO_2-water solution is cooled down until the hydrate formation conditions are attained. The growth rate of hydrates on the wall of the heat exchanger has been derived from the variation of the overall heat transfer coefficient with time. Results show that the addition of AFPs changes the supersaturation degree of CO_2 water solution needed to initiate the hydrate formation process.

A low concentration of the proposed additives is sufficient to slow down the formation rate of CO_2 hydrate improving significantly the controllability of the hydrate production process.

1. INTRODUCTION

The depletion of the ozone layer and the emission of greenhouse gases are two major environmental issues which pose great concerns to mankind and specifically to the refrigeration industry. Both environmental concerns and legal safety requirements force the search for new ways to phase out the potent greenhouse gases. One of the possible contributions to the reduction of these emissions is by reducing the quantity of primary refrigerants by utilizing secondary fluids. Primary refrigerants such as CFCs and HCFCs have been or are being phased out in compliance with the Montreal Protocol. Also HFCs are being limited due to their significant contribution to global warming.

Phase change materials (PCMs) can be used as secondary fluids which undergo a phase change from solid to liquid or liquid to gas or vice versa. Clathrate hydrate slurry consisting of water and fine solid clathrate particles is a promising candidate PCM for rapid chilling of fresh products. CO_2 hydrate slurry is a favourable secondary fluid which can be applied in direct contact to fresh products: it has a large latent heat (507 kJ/kg) and positive phase change temperature (4-8 °C). This allows for the application of primary refrigeration cycles which operate at significantly higher evaporating temperatures than cycles applied in conventional rapid chilling plants. The refrigeration cycle efficiency is correspondly significantly higher than usual.

There are three types of AFPs which have been isolated from the body fluids of many species of polar fish. AFPs are classified on the basis of their composition and tertiary structures (Sonnichsen et al., 1995). AFPs are environmental friendly additives that are able to prevent hydrate growth (Zeng et al., 2003) by binding to the surface of hydrate nuclei (Kelland, 2006) acting as kinetic inhibitors of crystal growth.

This study investigates the influence of AFPs on the formation rate of CO_2 hydrate. The results are relevant when continuous production of CO_2 hydrate slurry is to be developed.

2. EXPERIMENT

2.1 Experimental apparatus

Figure 1 shows a schematic diagram of the experimental setup. The system contains two thermostatic baths with two coil heat exchangers, a gear pump, two vessels (not shown), two glass windows and a range of sensors. The sensors are placed before and after the cold bath where the hydrates will form. The flow is circulated with the gear pump (0.37 kW) with adjustable speed and visualized from the two sight glasses. The water is ultra deionized water.

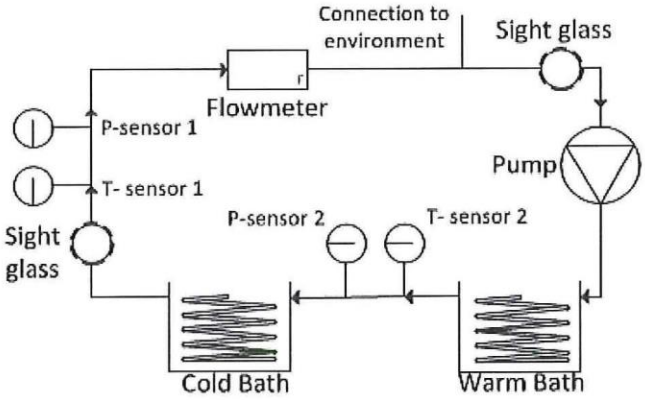

Figure 1: Set-up for CO_2 hydrate formation.

2.1 Experimental method

After the system has been brought to vacuum the CO_2 water solution with or without the addition of AFPs is added. The system is cooled by the thermostatic bath filled with water from 10°C with steps of 0.5 K until there are crystals appearing in the sight glasses. The effective cooling capacity of each bath is 0.3 kW. The second thermostatic bath (warm bath) is kept about 1 K higher than the first one (cold bath). Temperature of the fluids is measured at the inlet and outlet of the cold coil heat exchanger by PT100 temperature sensors. Two pressure sensors are located before and after the coil heat exchanger in the cold thermostatic bath to measure the pressure drop. The density is measured with a Coriolis mass flow meter. Temperatures, pressures, flow rate and density are stored every 5 seconds by a data logger.

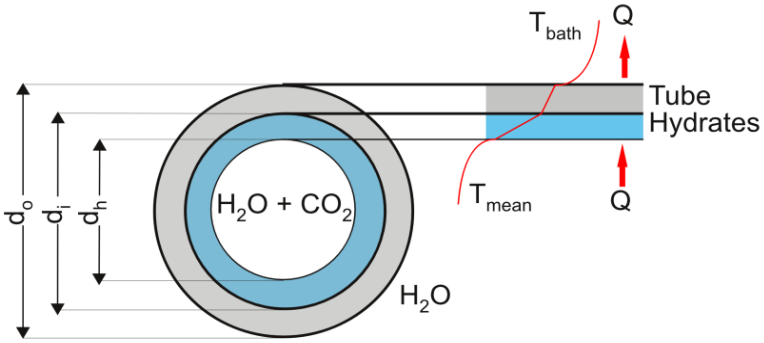

Figure 2: Hydrate formation on the wall of the coil. tubes

It's assumed that the hydrate crystals will firstly form on the wall of the tube located in the cold bath, which will increase the thermal resistance of the system, as depicted in Figure 2.

The experimental overall heat transfer coefficient of the system is calculated based on the measured temperatures, pressures and flow rates

$$U_{\exp} = \frac{\dot{m}\,\Delta i - \dot{m}\,\frac{\Delta P}{\rho_s} - \dot{Q}_{loss}}{A\Delta T_{\ln}} \tag{1}$$

Where $\Delta T_{\ln}$ is defined as

$$\Delta T_{\ln} = \frac{(T_{inlet} - T_{bath}) - (T_{outlet} - T_{bath})}{\ln \frac{T_{inlet} - T_{bath}}{T_{outlet} - T_{bath}}} \tag{2}$$

The energy loss in Eq. 1 equals to 3 W .

The overall heat transfer coefficient from the model without hydrates formation is calculated by Equation (3)

$$\frac{1}{U} = \frac{1}{h_o} + \frac{d_o \ln \frac{d_o}{d_i}}{2k_w} + \frac{d_o}{d_i}\frac{1}{h_i} \tag{3}$$

Equation (4) is used to calculate the overall heat transfer coefficient after hydrate crystals are formed

$$\frac{1}{U_h} = \frac{1}{h_o} + \frac{d_o \ln \frac{d_o}{d_i}}{2k_w} + \frac{d_i \ln \frac{d_i}{d_h}}{2k_h} + \frac{d_o}{d_h}\frac{1}{h_i} \tag{4}$$

Previous studies have shown that the outer heat transfer coefficient from the thermostatic bath is best predicted with the correlation of Churchill and Chu (1975)

$$Nu_o = 0.36 + \frac{0.518 * Ra^{1/4}}{(1 + (\frac{0.559}{\Pr})^{9/16})^{4/9}} \tag{5}$$

Similarly inner heat transfer coefficient is best predicted with the equation of Edwards et al. (1979)

$$Nu_s = 3.66 + \frac{0.065\frac{d_i}{L_c}\mathrm{Re}\Pr}{1 + 0.04\left(\frac{d_i}{L_c}\mathrm{Re}\Pr\right)^{2/3}} \tag{6}$$

3. RESULTS

3.1 Phase equilibrium of CO_2+H_2O hydrate

Diamond and Akinfiev (2003) investigated the CO_2 solubility in water. Yang et al. (2000) measured the phase equilibrium for CO_2+H_2O in hydrate formation conditions (shown in Figure 3). Hydrates can only be formed on the left side of point Q2. The supersaturation degree at hydrate formation is defined as

$$\Delta T = T_{eq} - T_{\exp}$$

The degree of supersaturation is quite an important factor to determine the initialization of hydrate formation. The supersaturation of CO_2 solution at hydrate formation with and without the addition of Type-III AFPs in different concentrations will be experimentally investigated.

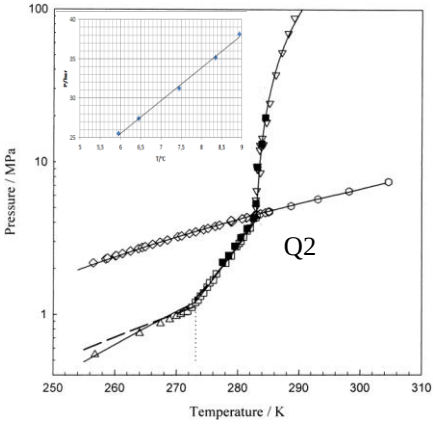

Figure 3: Phase equilibrium of CO_2-H_2O hydrate. From Yang et al. (2000).

3.2 Experiments

3.2.1 Set-up calibration

Before the system is applied for the experimental research, it's necessary to calibrate the system to make sure that it's accurate enough for the current work.

The calibration experiments were done with CO_2 water solution inside the tube. Figure 4 and Figure 5 show the temperature and pressure change with time. In the whole process, the condition of the solution is out of the hydrate formation region which can be derived from Figure 3. The wall temperature has been derived from the internal heat flux, with Equations (5) and (6).

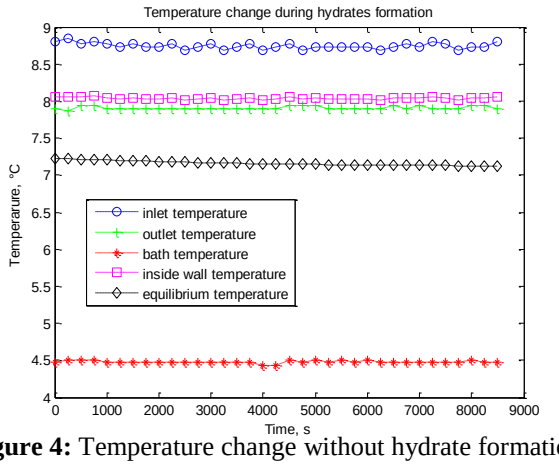

Figure 4: Temperature change without hydrate formation.

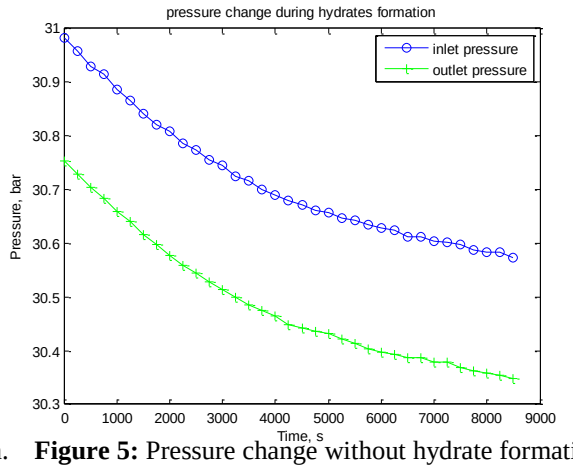

Figure 5: Pressure change without hydrate formation.

The overall heat transfer coefficient is predicted with Equation 3, in which the external and internal heat transfer coefficients are obtained with Equations (5) and (6). Figure 6 shows a comparison between the predicted and experimental values which are obtained from Equation (1).

The deviation is attributed to the prediction of the natural convection heat transfer coefficient outside the coil. The experimental data have been used to determine the average values of the coefficients of Equation (7).

$$Nu_o = 0.36 + a \times Ra^b \qquad (7)$$

Figure 7 shows the comparison of the overall heat transfer coefficient derived when Equation (5) is substituted by Equation (7) with coefficients a = 0.58 and b = 0.2.

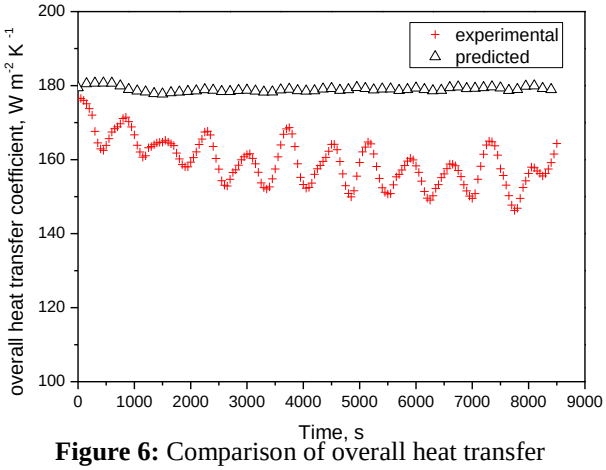

Figure 6: Comparison of overall heat transfer coefficient experimental and predicted with Equation (5).

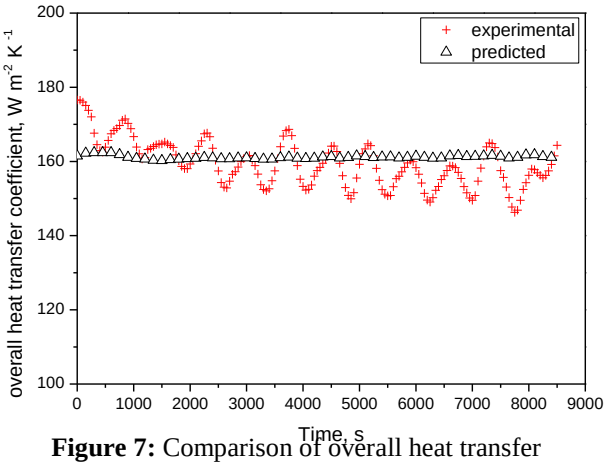

Figure 7: Comparison of overall heat transfer coefficient experimental and predicted with Equations (6) and (7).

3.2.2 Hydrate formation without the addition of AFPs

CO_2 hydrate formation experiments were done firstly without the addition of AFPs. Figure 8 and Figure 9 present the temperature and pressure change during the cooling down of CO_2 water solution. Figure 8 shows that the temperature of solution is cooled down gradually from the beginning. When the inside temperature reached about 7.0 °C and pressure was about 30 bar, temperature started increasing while the pressure in the inlet jumped from 30 bar to 40 bar suddenly.

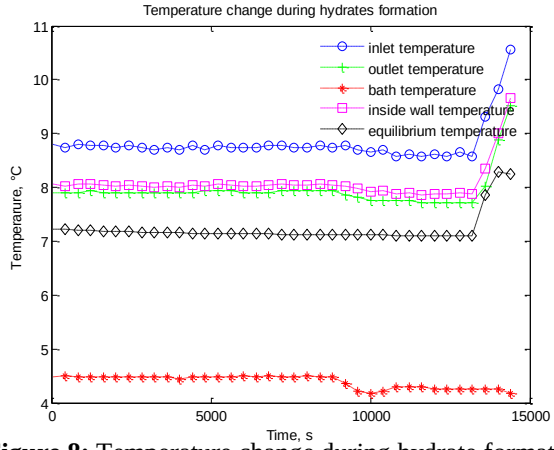

Figure 8: Temperature change during hydrate formation without the addition of AFPs.

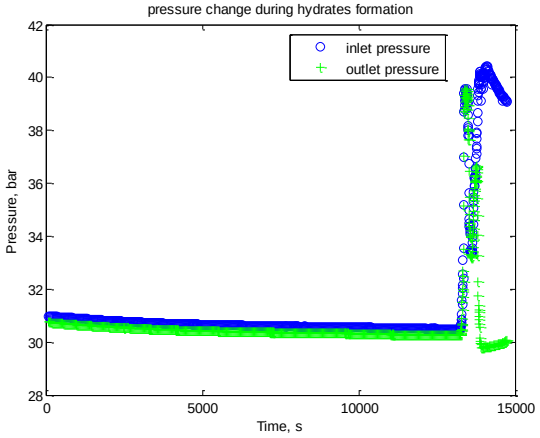

Figure 9: Pressure change during hydrate formation without the addition of AFPs.

With Equation (7), the overall heat transfer coefficient is predicted with a=0.58 and b=0.2. Hydrate diameter is then derived from Equation (1), Equation (4) and Equation (6).

Figure 10 shows during hydrate formation conditions the experimental and predicted overall heat transfer coefficient which show a reasonable match when there are no hydrates formed. Combining with Figure 11, it seems that there is no hydrate formation until 13200 seconds when a large amount of hydrates were formed and the pipes were blocked quite soon.

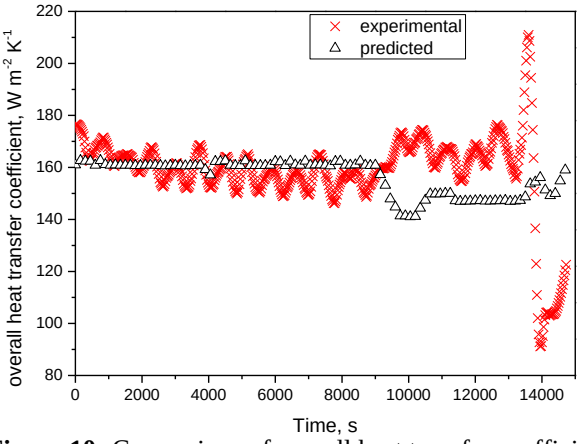

Figure 10: Comparison of overall heat transfer coefficient experimental and predicted with Equations (6) and (7).

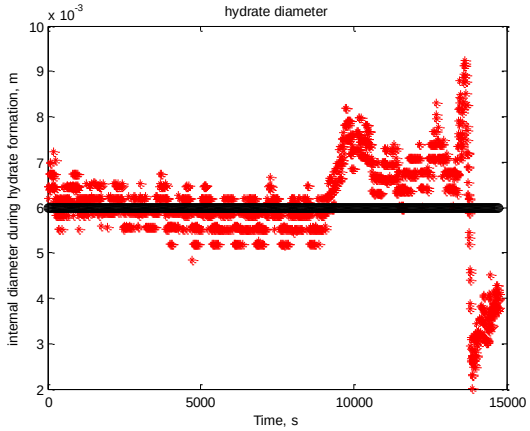

Figure 11: Hydrate diameter change with Equations (1), (4), (6) and (7).

3.2.3 Hydrate formation with the addition of 5 ppm AFPs

Figure 12 and Figure 13 show the temperature and pressure change during CO_2 water solution cooling down with the addition of 5 ppm AFPs in weight percent. The temperature was lowered gradually until a blockage took place.

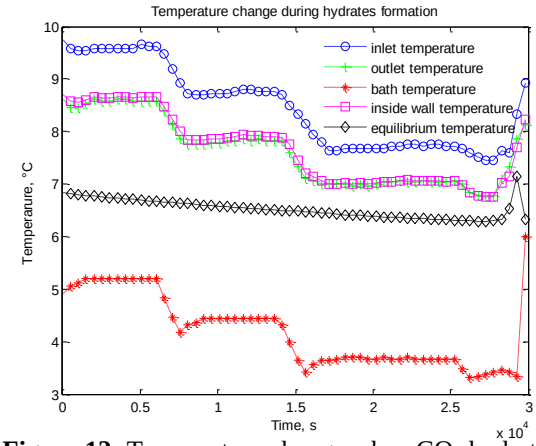

Figure 12: Temperature change when CO_2 hydrate formed with 5 ppm AFPs.

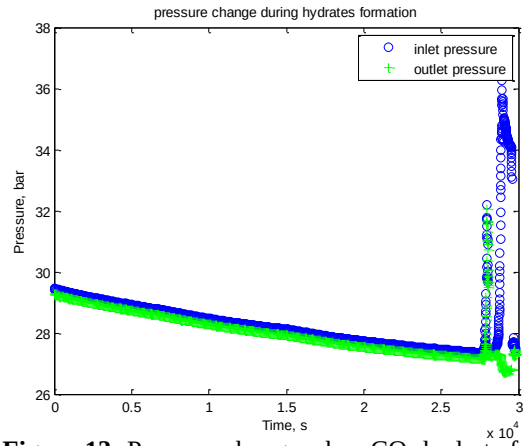

Figure 13: Pressure change when CO_2 hydrate formed with 5 ppm AFPs.

When the coefficients of Equation (7) are a = 0.58 and b = 0.2, the comparison of the overal heat transfer coefficient is shown in Figure 14. The deviation is attributed to the calculation of the internal heat transfer coefficient.

When Equation (6) is modified to

$$Nu_s = 2.6 + \frac{0.065\frac{d_i}{L_c}\mathrm{Re}\,\mathrm{Pr}}{1 + 0.04\left(\frac{d_i}{L_c}\mathrm{Re}\,\mathrm{Pr}\right)^{2/3}} \qquad (8)$$

there is a good match of the predicted and experimental values of the overall heat transfer coefficient, which can be seen from Figure 15. The second part of Equation (8) is quite small compared with the first part, therefore, in this case, by using Equation (8) the inside heat transfer coefficient is reduced by about 30% due to the addition of AFPs.

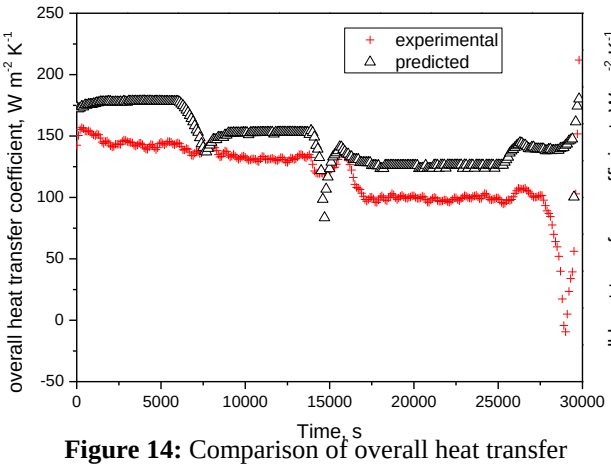

Figure 14: Comparison of overall heat transfer coefficient with 5 ppm AFPs experimental and predicted with Equations (6) and (7).

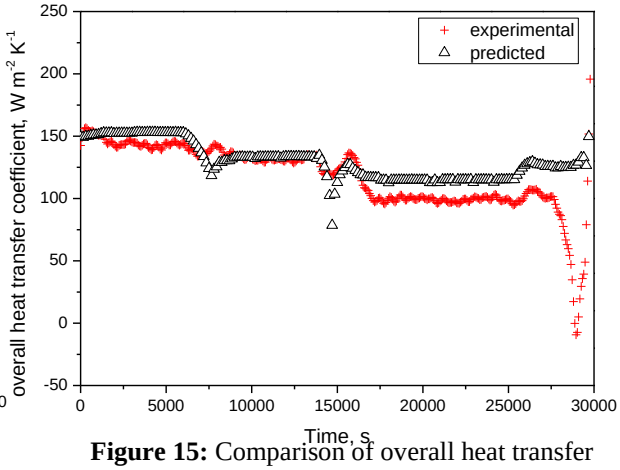

Figure 15: Comparison of overall heat transfer coefficient with 5 ppm AFPs experimental and predicted with Equations (7) and (8).

Then the hydrate diameter is calculated as a function of time by using of Equation (1) and Equation (4).

It can be seen from Figures 15 and 16 that hydrates started forming from about 14000 seconds, while there were no crystals visible in the sight glasses mentioned above. Therefore, it's assumed that the hydrate crystals are possibly formed on the wall of the tube in the cold bath firstly. There was a sharp temperature decrease at 14000 seconds, that possibly caused the crystal formation. From then on, hydrates formed until about 29000 seconds when the pipe was blocked. This can be seen from Figure 16 that shows that the hydrate diameter reduced to almost zero.

Figure 12 shows that at the moment hydrates started forming the difference between the inside wall temperature and the equilibrium temperature is quite small (0.3 K). It means that the addition of 5 ppm doesn't change too much the supercooling degree of the CO_2 solution.

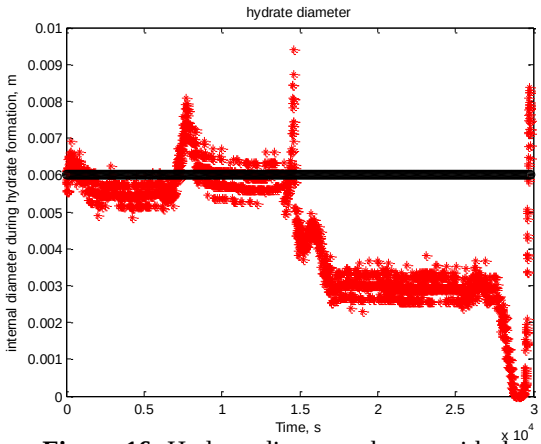

Figure 16: Hydrate diameter change with the addition of 5 ppm AFPs.

The hydrate growth rate can be derived from Figure 16 by using Equation (9). The average growth rate is 0.0346 kg/h from 14000 seconds to 29000 seconds. The hydrates formed rapidly in the beginning and then kept stable until the pipe was blocked.

$$G_h = \frac{\rho_h \pi (d_i^2 - d_h^2) L_c}{4 \Delta t} \tag{9}$$

The average hydrate growth rate is about 0.5 μm/s during the time from 14000 seconds to 17000 seconds while the supercooling was initially about 0.3 K.

$$v = \frac{d_i - d_h}{\Delta t} \tag{10}$$

While the hydrate growth rate derived from Uchida et al. (2002) by Equation (10) when the supercooling degree equals to 0.3 K is 0.519 mm/s.

$$v_{Uchida} = 1.73 \times 10^{-3} \Delta T \tag{11}$$

3.2.4 Hydrate formation with the addition of 10 ppm AFPs

Figure 17 and Figure 18 show the temperature and pressure change during hydrate formation with the addition of 10 ppm AFPs. The solution is cooled down from about 10 °C in steps until there is a sharp increase accompanied by a sudden rise of pressure.

Similarly to the previous case, when the coefficients of Equation (7) have been modified as a = 0.58 and b = 0.2, and the internal heat transfer coefficient is calculated by Equation (8), the values of the experimental and predicted overall heat transfer coefficient show a good match, which can be seen from Figure 19. The hydrate diameter is calculated as a function of time by using Equations (1), (4), (7) and (8).

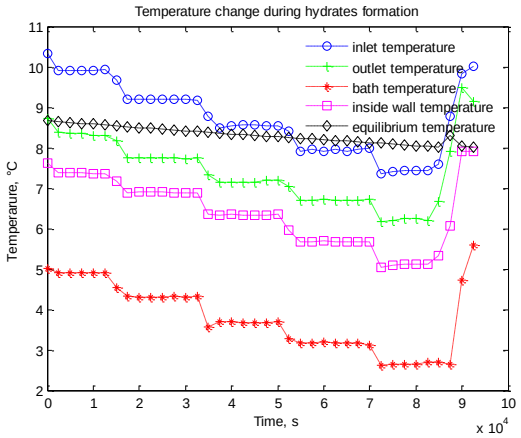

Figure 17: Temperature change when CO_2 hydrate formed with 10 ppm AFPs.

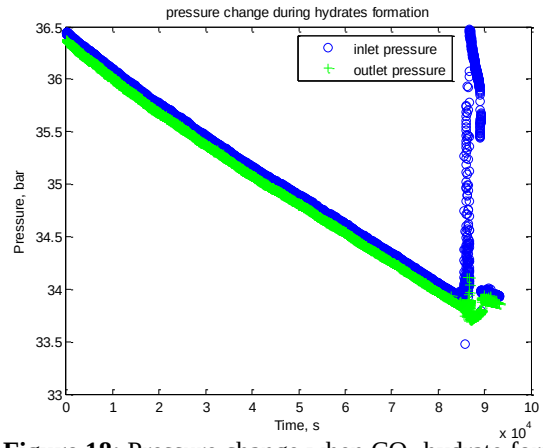

Figure 18: Pressure change when CO_2 hydrate formed with 10 ppm AFPs.

Figure 19 and Figure 20 show that from about 52000 seconds (14.4 hours) on, a deviation between the experimental and predicted overall heat transfer coefficient starts to appear. But the hydrate diameter decreased suddenly at about 35000 seconds, and kept constant until it went down again from 52000 seconds. it's possibly because the sharp decrease at 35000 seconds seen from Figure 17 which induced the first decrease. Therefore, hydrate is assumed to start forming from 52000 seconds, with inside wall temperature 6.2℃ and pressure 35.3 bar. While the equilibrium temperature at 35.3 bar is about 8.3℃. Then the supercooling degree with the addition of 10 ppm AFPs is 2.1 K as the first crystals are formed.

The average hydrate growth rate from Figure 20 derived from Equation (9) is 0.010 kg/h from 35000 seconds to 85000 seconds. The hydrate thickness growth rate derived by using Equation (10) is about 0.033μm/s when the hydrate started forming at initial supercooling degree of 2.1 K, while the growth rate obtained from Equation (11) is 3.63 mm/s at supercooling degree of 2.1 K.

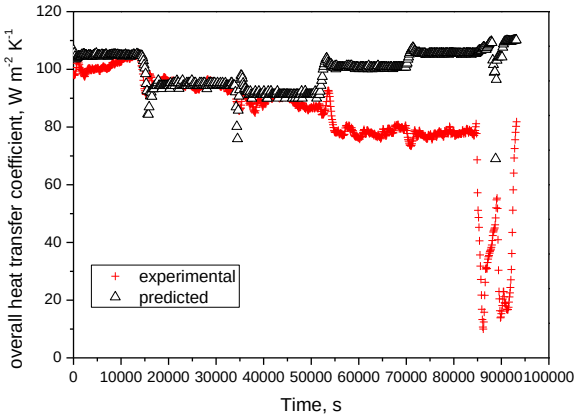

Figure 19: Comparison of overall heat transfer coefficient with 10 ppm AFPs experimental and predicted with Equations(7) and (8).

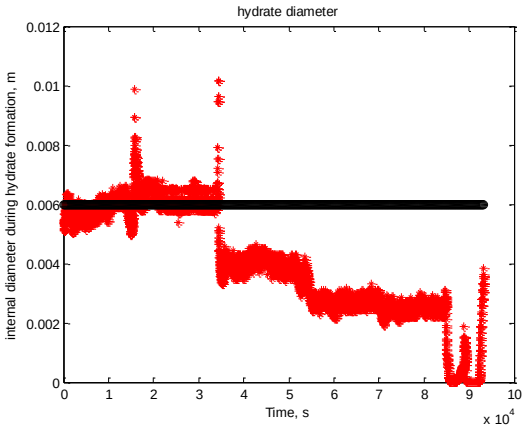

Figure 20: Hydrate diameter change with the addition of 10 ppm AFPs.

3.3 Discussion

Table 1 summarizes the influence of AFPs on CO_2 hydrate formation compared with the results from Uchida et al. (2002). It indicates that the supercooling degree of CO_2 hydrate formation is influenced significantly when the concentration of AFPs is 10 ppm, while with 5 ppm AFPs there was almost no effect on the supercooling degree.

The hydrate formation rate can be derived when there is an addition of AFPs in the solution, and it's signigicantly lowered down with the addition of AFPs.

Table 1: Influence of AFPs on hydrate formation varies with concentration

Concentration of AFPs / ppm	$h_{iwith}/h_{iwithout}$	Supercooling / K	Growth rate / (kg/h)	Formation rate (Eq. 9/Eq. 10) / (mm/s)
0	1.00	—	—	—
5	0.72	0.3	0.0346	0.5e-3/0.519
10	0.72	2.1	0.01	0.033e-3/3.63

The experiments have indicated that the addition of AFPs to the CO_2-water solution also reduces significantly the heat transfer coefficient which can be seen from Table 1.

4. CONCLUSIONS

The addition of Type-III AFPs changes the CO_2 hydrate formation behaviour. With the addition of 10 ppm AFPs in weight percent, the supercooling degree is increased a lot compared with that without the addition of AFPs. The addition of 5 ppm AFPs has a much smaller effect.

With the addition of 5 ppm and 10 ppm AFPs, the hydrate production rate can be determined. While in the case without the addition of AFPs the growth rate is too large so that its rate cannot be determined from the present experiments.

NOMENCLATURE

A	Area	m^2	ν	Film growth rate	$m\ s^{-1}$

d	Diameter	m	π	Pi	
h	Heat transfer coefficient	W m^{-2} K^{-1}	ρ	Density	kg m^{-3}
i	Enthalpy	J kg^{-1}	**Subscript**		
k	Thermal conductivity	W m^{-1} K^{-1}	bath	Bath	
L	Length	m	c	Coil	
ṁ	Mass flowrate		eq	Equilibrium	
Nu	Nusselt number		exp	Experimental	
P	Pressure	Pa	h	Hydrate	
Pr	Prantl number		i	Inner	
$\dot{Q}$	Energy flow	J s^{-1}	inlet	Inlet	
Ra	Rayleigh number		ln	Logarithmic	
Re	Reynolds number		loss	Loss	
T	Temperature	K	mean	Mean	
t	Time	s	o	Outer	
U	Overall heat transfer coefficient	W m^{-2} K^{-1}	outlet	Outlet	
Greek			s	Slurry	
Δ	Difference		w	Wall	

REFERENCES

Churchill, S.W., Chu, H.H.S., 1975, Correlating equations for laminar and turbulent free convection from a horizontal cylinder. *Int. J. Heat Mass Transfer*. vol. 18, p. 1049-1053.

Diamond, L.W., Akinfiev, N.N., 2003, Solubility of CO_2 in water from -1.5 to 100 °C and from 0.1 to 100 MPa: evaluation of literature data and thermodynamic modelling, *Fluid Phase Equilibria*, vol. 208, p. 265-290.

Edwards, D.K., Denny, V.E., Mills, A.F., 1979, *Transfer Processes*, 2nd ed., Hemisphere, Washington, D.C..

Kelland, M.A. , 2006, History of the development of low dosage hydrate inhibitors, *Energy Fuels* 20, p. 825–847.

Sonnichsen, F.D., Sykes, B.D., Davies, P.L., 1995, Comparative modelling of the 3-dimensional structure of type-II antifreeze protein, *Protein Sci*. vol. 4, no. 3 : p. 460–471.

Uchida, T., Ikeda, I.Y., Ebinuma, T., Nagao, J., Narota, H., 2002, CO_2 hydrate film formation at the boundary between CO_2 and water: effects of temperature, pressure and additives on the formation rate, *Journal of Crystal Growth*, p.383-387.

Yang, S.O., Yang, I.M., Kim, Y.S., Lee,C.S., 2000, Measurement and prediction of phase equilibria for water+CO_2 in hydrate formation conditions, *Fluid Phase Equilibria*, vol.175, p.75-89.

Zeng, H., Wilson, L.D. , Walker, V.K. , Ripmeester, J.A. , 2003, The inhibition of tetrahy- drofuran clathrate-hydrate formation with antifreeze protein, *Can. J. Phys*, vol.81, p. 17–24.